Direct Measurement of the Binding Energy and Bohr Radius of a Single Hydrogenic Defect in a Semiconductor Quantum Well

Simon Perraud,[1,2] Kiyoshi Kanisawa,[1,*] Zhao-Zhong Wang,[2] and Toshimasa Fujisawa[1]

[1]*NTT Basic Research Laboratories, NTT Corporation, Atsugi, Kanagawa 243-0198, Japan*

[2]*Laboratoire de Photonique et de Nanostructures, CNRS, 91460 Marcoussis, France*

(Received 15 August 2007; published 7 February 2008)

Low-temperature scanning tunneling spectroscopy under ultrahigh vacuum was used to study donor point defects located at the epitaxial surface of an $In_{0.53}Ga_{0.47}As$ quantum well. The electronic local density of states was measured with nanoscale resolution in the vicinity of single defects. In this way, both the binding energy and the Bohr radius of the defects could be determined. The binding energy and the Bohr radius were found to be functions of the quantum well thickness, in quantitative agreement with variational calculations of hydrogenic impurity states.

DOI: 10.1103/PhysRevLett.100.056806 PACS numbers: 73.20.Hb, 73.21.Fg, 73.61.Ey

Doping a semiconductor with foreign atoms called impurities allows to precisely tune the concentration of charge carriers, a principle at the basis of virtually all electronic and optoelectronic devices [1]. In the simplest approximation, an impurity inside a semiconductor is described as an hydrogen atom [1]. Thus the two essential properties of an impurity are the binding energy and the Bohr radius. Up to now, only the binding energy can be determined experimentally, by techniques such as absorption, luminescence, and Raman scattering [2]. However, it is highly desirable to also measure the Bohr radius a_B, which is a key parameter for various phenomena, e.g., an impurity band is formed if $a_B \gtrsim s$, where s is the mean impurity separation [3]; two impurity nuclear spins interact if $a_B \gtrsim d$, where d is the distance between impurities [4]; impurities in quantum wells (QWs) are affected by the confining potential if $a_B \gtrsim l$, where l is the QW thickness [5]. The case of an impurity in a QW has attracted considerable attention [6], since it is a model system for an hydrogen atom in reduced dimensionality [7].

Here, we use scanning tunneling microscopy and spectroscopy (STM, STS) to study point defects behaving like donor impurities, which are located at the epitaxial surface of a QW. By measuring with nanoscale resolution the electronic local density of states (LDOS) in the QW, we are able to determine both the binding energy and the Bohr radius of single defects. Moreover, we show that the binding energy and the Bohr radius depend on the QW thickness, in quantitative agreement with the hydrogenic model. Note that some aspects of the physics of impurities in semiconductors have been already investigated by STM [8], but there has been so far no systematic measurement of binding energy and Bohr radius allowing a precise comparison with the hydrogenic model.

(111)*A*-oriented, nominally undoped $In_{0.53}Ga_{0.47}As$ surface QWs were grown by molecular beam epitaxy (MBE). The sample structure has been described elsewhere [9]. Four different QW thicknesses were investigated in this work ($l = 2$, 6, 10, and 14 nm). After the growth, samples were transferred under ultrahigh vacuum (UHV) to a low-temperature STM chamber and cooled down to 5 K. STM topographic images were acquired in the constant-current mode. For STS experiments, a sinusoidal modulation ($U_{\mathrm{mod}} = 10$ mV peak-to-peak, $f_{\mathrm{mod}} = 700$ Hz) was added to the sample voltage U, and the differential conductance dI/dU was measured through a lock-in amplifier. dI/dU at U is proportional to the LDOS at the sample surface at

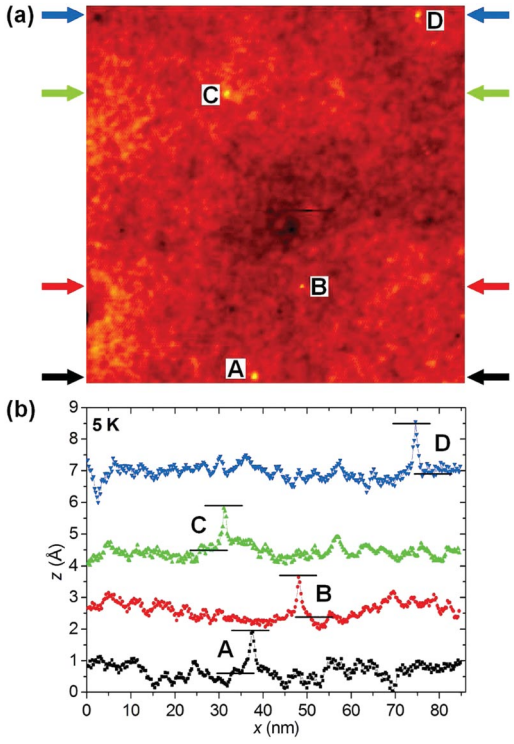

FIG. 1 (color). (a) 85.3×85.3 nm^2 STM topography ($U = +1.1$ V; $I = 0.1$ nA) of the QW surface, for $l = 6$ nm. Four point defects are visible (bright spots), and denoted by A, B, C, and D. (b) Height profiles along the horizontal lines indicated by arrows in (a), running through the point defects.

energy $+eU$ ($U = 0$ corresponds to the Fermi level), if the tip-sample distance is constant.

Figure 1(a) shows a STM topography of the QW surface. The mottled appearance of the image is due to local fluctuations of the InGaAs alloy composition [10]. Four point defects are visible, appearing as protrusions for $U > 0$, with a corrugation of $0.15(\pm 0.02)$ nm at $U = +1.1$ V as shown in Fig. 1(b) [11]. The density of the defects at the QW surface, which is less than 1.5×10^{11} cm^{-2}, does not increase with time. Therefore the defects are not due to surface contamination by residual gas atoms in the UHV environment of the STM chamber, but are rather native defects formed during the MBE growth [12]. Furthermore, as shown below, the defects behave like donor impurities. First-principle calculations suggest that such donor native point defects observed at the $In_{0.53}Ga_{0.47}As(111)A$ surface are Ga (or In) adatoms sitting on top of the surface [13].

In the STM topography of Fig. 2(a), a single point defect is visible, with no other defects in the vicinity. A dI/dU spectrum was acquired on each pixel of a 64×64 grid of the area of Fig. 2(a), for U ranging from 0 V to +1 V [conduction band (CB) region]. Figure 2(b) shows the dI/dU spectra averaged over rings of thickness 1 nm and of several radii r, centered on the defect. The dI/dU spectrum at $r = 9.7$ nm has a steplike voltage dependence, as expected for a two-dimensional (2D) electronic system [14]. The steps correspond to the subbands formed in the QW due to quantum confinement along the growth direction. The dI/dU spectrum at $r = 9.7$ nm also exhibits a peak below each subband minimum. The height of these peaks increases as r decreases. The peak found below the nth subband minimum is interpreted as a bound state splitting off from the nth subband, due to an attractive potential created by the defect [15]. In other words, the defect behaves like a donor impurity. Bound states splitting off from a 2D continuum have been recently observed by STS measurements on metal surface states [16]. In contrast with those works, here it is possible to study the influence of quantum confinement on the bound states, by simply varying l.

Note that two features of unknown origin are observed in Fig. 2(b). First, the bound state peaks move to lower U when r increases. Since this shift has a small amplitude (about 10 mV between $r = 0.9$ nm and $r = 9.7$ nm, which is comparable to U_{mod}), it will be neglected in the following. At $r = 0.9$ nm, the bound states are located at $U = \varepsilon_1$, ε_2, and ε_3. Second, a peak which is not related to a bound state splitting off from a subband is found at $U = E_A$. This peak only appears for $r < 2$ nm (i.e., in the immediate vicinity of the defect), while the bound state peaks can be observed up to $r \approx 13$ nm. For all the defects, E_A is $0.5(\pm 0.05)$ eV above the CB minimum, independently of l.

Figure 2(c) shows the dI/dU spatial maps at $U = \varepsilon_1$, ε_2, and ε_3. The wave functions of the bound states are not completely isotropic, but are slightly elongated in one

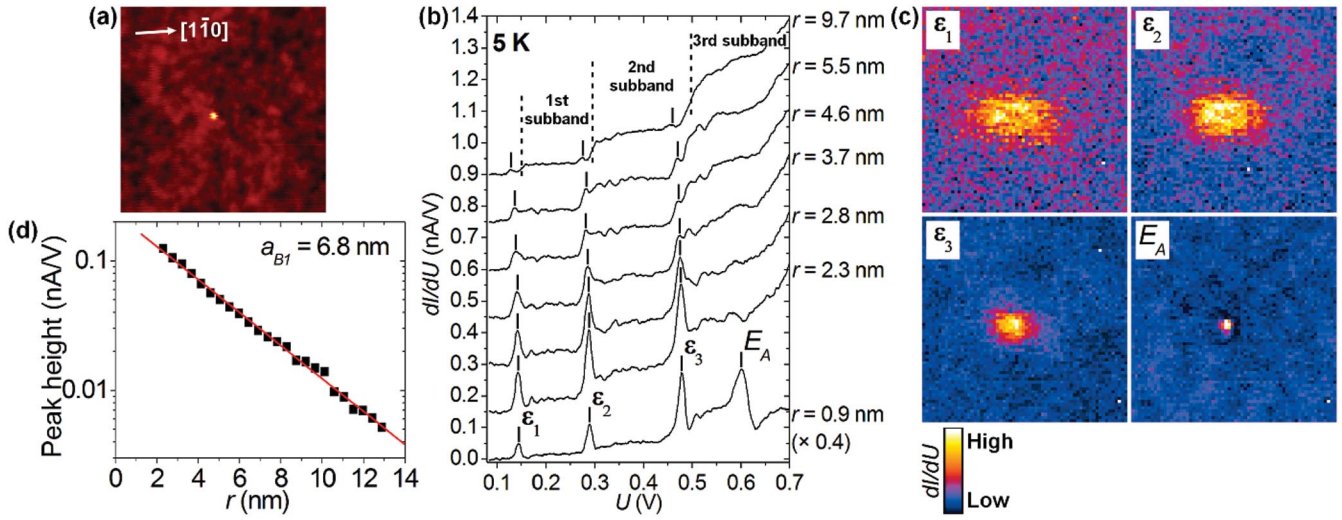

FIG. 2 (color). Determination of the Bohr radius of a single point defect at the QW surface, for $l = 10$ nm. (a) 29.5×29.5 nm^2 STM topography ($U = +1.1$ V; $I = 0.5$ nA). A point defect (bright spot) is visible. A dI/dU spectrum was acquired simultaneously to the STM topography, on each pixel of a 64×64 grid, for U ranging from 0 V to +1 V (CB region). (b) dI/dU spectra averaged over rings of thickness 1 nm and of several radii r, centered on the defect (for clarity, the spectra are offset by a constant of 0.15 nA/V, relative to the lowest curve; the ordinate axis for the spectrum at $r = 0.9$ nm is multiplied by 0.4). Three subbands are observed in the present case where $l = 10$ nm, in agreement with the calculations detailed in the text. A peak is found below each subband minimum, as indicated by vertical lines. For the dI/dU spectrum at $r = 0.9$ nm, these peaks are found at $U = \varepsilon_1$, ε_2, and ε_3. (c) dI/dU spatial maps of the same area as in (a), at several values of U indicated in (b). (d) Height of the dI/dU peak attached to the first subband as a function of distance r from the defect (squares). Also shown is a fit by an exponential decay $A \exp(-2r/a_{B1})$ (solid line). The fit leads to the Bohr radius for the first subband, $a_{B1} = 6.8(\pm 1)$ nm. Note that the ordinate axis has a logarithmic scale.

particular direction. The exact shape of the wave functions was found to vary from defect to defect, with no clear relation to the crystal symmetry. This is consistent with the fact that a disorder potential has been observed in the QW [9]. The disorder potential, superimposed on the central potential of the defect, induces a small distortion of the wave functions of the bound states.

The spatial extension of the wave functions of the bound states can be precisely determined by plotting the height of the corresponding dI/dU peaks as a function of r. Figure 2(d) shows the case of the bound state attached to the first subband [17]. The obtained spatial dependence is well fitted by an exponential decay $A\exp(-2r/a_{B1})$, representing the 1 s hydrogenic wave function. The fit leads to the Bohr radius for the first subband, $a_{B1} = 6.8(\pm 1)$ nm. The Bohr radii determined in a similar way for high-order subbands are $a_{B2} = 6.1(\pm 1)$ nm and $a_{B3} = 5.4(\pm 1)$ nm.

Having shown how to determine the Bohr radius of a point defect, we now present a method for determining the binding energy. The binding energy is defined as the difference between the energy of the bound state and that of the subband minimum. On one hand, the bound state peaks appear the most clearly in the dI/dU spectra acquired close to the defect. Therefore, the bound state energies ε_n were determined from the dI/dU spectrum at the smallest measured radius, $r = 0.9$ nm. On the other hand, the steps associated with the subband minima appear the most clearly in the dI/dU spectra acquired far from the defect. From about $r = 2a_{B1}$, the dI/dU spectra exhibit a clear steplike voltage dependence, the bound state peaks having completely vanished. Therefore the subband minima E_n were determined from the dI/dU spectrum at $r = 2a_{B1}$ (for a precise determination of the energy position of the steps, the derivative of the dI/dU spectrum at $r = 2a_{B1}$ was calculated and then fitted by Gaussian functions). The binding energy for the nth subband is then given by $E_n - \varepsilon_n$. Figure 3 illustrates this method for three different values of l.

Figure 4 summarizes the STS data obtained in this work. The smaller l, the larger $E_1 - \varepsilon_1$, and the smaller a_{B1}, i.e., the tighter the electron is bound to the point defect. Thus we clearly observe the influence of quantum confinement on the bound states, as expected in the present case $a_{B1} \gtrsim l$ [5]. Note that for a given value of l, different defects do not have exactly the same $E_1 - \varepsilon_1$ or the same a_{B1}. As mentioned above, this can be explained by the presence of a disorder potential in the QW [9,18].

Let us now compare the STS data with a calculation of hydrogenic impurity states. The effect of tip-induced band bending on the bound states was neglected [19]. However, the CB nonparabolicity was taken into account, since it plays a significant role in $In_{0.53}Ga_{0.47}As$ [10]. The method proposed in Ref. [20] was employed. It consists of two steps. In the first step, the energies E_n were determined with respect to the CB minimum by solving the one-dimensional Schrödinger equation in the $In_{0.53}Ga_{0.47}As$ QW, with a CB dispersion relation given by a two-band Kane model including nonparabolicity [21], and an effective mass at the CB minimum of $0.041m_0$ [22]. This calculation has been described in detail elsewhere [9]. For a given value of l, the number of subbands found by solving the Schrödinger equation agrees with the STS data. In the second step, $E_1 - \varepsilon_1$ and a_{B1} were determined by using a variational calculation for an electron bound to a point charge $+e$ [5]. The point charge was taken to be at the QW boundary, since the point defects are located at the

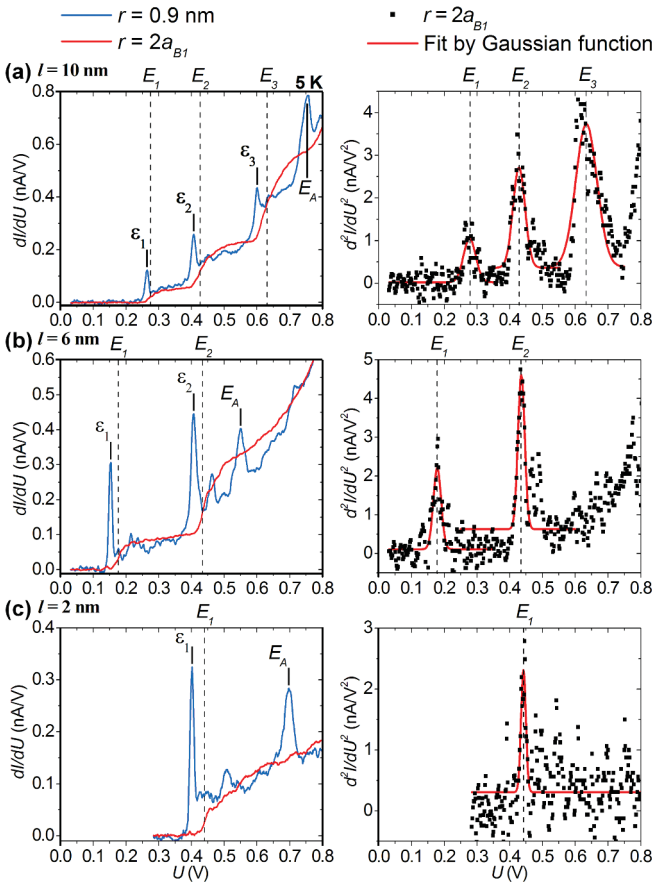

FIG. 3 (color). Determination of the binding energy of a single point defect at the QW surface. An analysis similar to that of Fig. 2 leads to the Bohr radius for the first subband a_{B1}. The energy of the bound state attached to the nth subband ε_n is determined from the dI/dU spectrum at $r = 0.9$ nm. The nth subband minimum E_n is determined from the d^2I/dU^2 spectrum at $r = 2a_{B1}$. The binding energy for the nth subband is then given by $E_n - \varepsilon_n$. (a) $l = 10$ nm, for a defect with $a_{B1} = 7.3(\pm 1)$ nm. (b) $l = 6$ nm, $a_{B1} = 5.15(\pm 1)$ nm. (c) $l = 2$ nm, $a_{B1} = 4.4(\pm 1)$ nm. Three subbands are observed for $l = 10$ nm, two subbands for $l = 6$ nm, and one subband for $l = 2$ nm, in agreement with the calculations detailed in the text. Note that the disorder potential in the QW [9] induces a rigid shift of subband minima when the spatial position changes. Therefore one can only compare the subband *spacings* in dI/dU spectra for different defects.

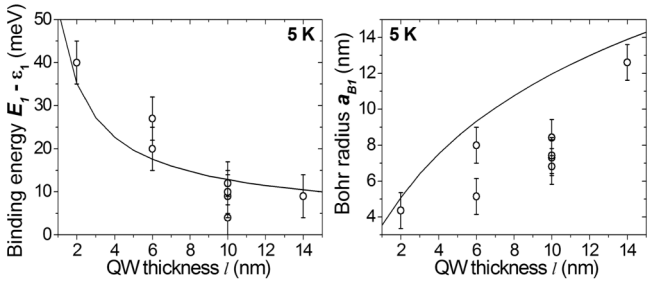

FIG. 4. Binding energy $E_1 - \varepsilon_1$ and Bohr radius a_{B1} as a function of QW thickness l: STS data (each circle corresponds to a single point defect at the $In_{0.53}Ga_{0.47}As$ QW surface), and hydrogenic model (solid curves).

QW surface. The dielectric constant was that for a point charge at the interface between $In_{0.53}Ga_{0.47}As$ and vacuum, given by $\frac{\epsilon_0+\epsilon_{\text{bulk}}}{2}$ [23] ($\epsilon_{\text{bulk}} = 13.75\epsilon_0$ is the dielectric constant of $In_{0.53}Ga_{0.47}As$ [1]). The electron effective mass was given by the two-band Kane model at the energy E_1 determined in the first step. The calculation agrees well with the STS data, as shown in Fig. 4. We emphasize that this calculation has no adjustable parameter. The increase of $E_1 - \varepsilon_1$ (or, equivalently, the decrease of a_{B1}) with decreasing l is enhanced by the CB nonparabolicity. From $l = 14$ nm to $l = 2$ nm, $E_1 - \varepsilon_1$ increases by factors 2.4 and 3.3 without and with considering the CB nonparabolicity, respectively.

We point out that the distribution of LDOS along the growth direction $|\psi_n(z)|^2$ depends on the subband index n [in the ideal case of a QW with infinite barrier height, $|\psi_n(z)|^2 \propto \sin^2(\frac{n\pi z}{l})$ where z is the distance from the QW boundary]. The distance between the QW boundary and the closest maximum of $|\psi_n(z)|^2$ decreases with increasing n (in the case of infinite barrier height, this distance is $l/2n$). Therefore the binding of the electron to a point defect located at the QW boundary is expected to become tighter for larger n. This is what is observed in the STS data of Figs. 2 and 3. Further experimental work is needed, e.g., by studying impurities at different positions along the growth direction.

In summary, STS was used to study donor point defects located at the surface of a semiconductor QW. Both the binding energy and the Bohr radius could be determined, and were found to depend on the QW thickness, in quantitative agreement with the hydrogenic model.

We gratefully acknowledge G. Bastard (Ecole Normale Supérieure, Paris) for fruitful discussions. This work was partly supported by JSPS KAKENHI (No. 16206003).

*kani@will.brl.ntt.co.jp

[1] S. M. Sze, *Semiconductor Devices* (Wiley, New York, 2002), 2nd ed.
[2] J. M. Baranowski and M. Grynberg, in *Handbook on Semiconductors*, edited by P. T. Landsberg (Elsevier, Amsterdam, 1992), Vol. 1, Chap. 5.
[3] P. Van Mieghem, Rev. Mod. Phys. **64**, 755 (1992).
[4] B. E. Kane, Nature (London) **393**, 133 (1998).
[5] G. Bastard, Phys. Rev. B **24**, 4714 (1981).
[6] For a review, see B. V. Shanabrook, Physica (Amsterdam) **146B+C**, 121 (1987).
[7] X. L. Yang *et al.*, Phys. Rev. A **43**, 1186 (1991).
[8] R. M. Feenstra *et al.*, Phys. Rev. B **66**, 165204 (2002); A. M. Yakunin *et al.*, Phys. Rev. Lett. **92**, 216806 (2004); G. Mahieu *et al.*, *ibid.* **94**, 026407 (2005).
[9] S. Perraud *et al.*, Phys. Rev. B **76**, 195333 (2007).
[10] S. Perraud *et al.*, Appl. Phys. Lett. **89**, 192110 (2006).
[11] The variation of corrugation from defect to defect is small (the error bar of ± 0.02 nm is comparable with the corrugation associated with the fluctuations of alloy composition), indicating that all the defects are located at the same position along the growth direction.
[12] Surface contamination during the sample transfer under UHV from the MBE chamber to the STM chamber is unlikely, since the transfer is fast (less than 20 min) and the surface is hot (more than 400 °C when the sample is taken out from the MBE chamber).
[13] A. Taguchi, K. Shiraishi, and T. Ito, Phys. Rev. B **60**, 11 509 (1999); A. Taguchi and K. Kanisawa, Appl. Surf. Sci. **252**, 5263 (2006).
[14] K. Suzuki *et al.*, Phys. Rev. Lett. **98**, 136802 (2007).
[15] C. Priester, G. Allan, and M. Lannoo, Phys. Rev. B **29**, 3408 (1984).
[16] F. E. Olsson *et al.*, Phys. Rev. Lett. **93**, 206803 (2004); L. Limot *et al.*, *ibid.* **94**, 036805 (2005).
[17] The dI/dU peak height is plotted for $r > 2$ nm. For $r < 2$ nm, the point defect is visible in the STM topography, hence the r dependence of dI/dU may reflect a variation of tip-sample distance.
[18] The disorder electric field and the donor point defect electric field are comparable, since they are of the order of magnitude of $2\sqrt{2\ln 2}V_{\text{rms}}(L)/eL \approx 0.5$ mV/nm [9] and $(E_1 - \varepsilon_1)/ea_{B1} \approx 1$ mV/nm, respectively ($l = 10$ nm).
[19] Tip-induced band bending [R. M. Feenstra and J. A. Stroscio, J. Vac. Sci. Technol. B **5**, 923 (1987)] was estimated by assuming that the unintentional n-type impurity density in the nominally undoped $In_{0.53}Ga_{0.47}As$ layer is about 1×10^{15} cm^{-3} [W. Lee and C. G. Fonstad, J. Vac. Sci. Technol. B **4**, 536 (1986)]. For $U > 0$, the space-charge layer thickness was found to be larger than 100 nm, hence much larger than a_{B1}.
[20] S. Chaudhuri and K. K. Bajaj, Phys. Rev. B **29**, 1803 (1984).
[21] E. O. Kane, in *Semiconductors and Semimetals*, edited by R. K. Willardson and A. C. Beer (Academic, New York, 1975), Vol. 1, Chap. 3.
[22] *Properties of Lattice-Matched and Strained Indium Gallium Arsenide*, edited by P. Bhattacharya, INSPEC-EMIS Datareview Series No. 8 (Institution of Electrical Engineers, London, 1993).
[23] J. D. Jackson, *Classical Electrodynamics* (Wiley, New York, 1975), 2nd ed., Sec. 4.4.